Journal of Power Sources 196 (2011) 2115–2121

Contents lists available at ScienceDirect

Journal of Power Sources

journal homepage: www.elsevier.com/locate/jpowsour

Polypropylene-supported and nano-Al_2O_3 doped poly(ethylene oxide)–poly(vinylidene fluoride-hexafluoropropylene)-based gel electrolyte for lithium ion batteries

Y.H. Liao [a], X.P. Li [a,b,c], C.H. Fu [d], R. Xu [d], L. Zhou [a], C.L. Tan [a,b,c], S.J. Hu [a,b,c], W.S. Li [a,b,c,*]

[a] School of Chemistry and Environment, South China Normal University, Guangzhou 510006, China
[b] Key Laboratory of Electrochemical Technology on Energy Storage and Power Generation of Guangdong Higher Education Institutes, South China Normal University, Guangzhou 510006, China
[c] Engineering Research Center of Materials and Technology for Electrochemical Energy Storage (MOE), South China Normal University, Guangzhou 510006, China
[d] Amperex Technology Limited, Dongguan 523080, China

ARTICLE INFO

Article history:
Received 23 July 2010
Received in revised form 20 October 2010
Accepted 21 October 2010
Available online 30 October 2010

Key words:
Nano-aluminum oxide
Poly(ethylene oxide)–poly(vinylidene fluoride-hexafluoropropylene)
Gel polymer electrolyte
Lithium ion battery
Polypropylene-supported

ABSTRACT

A new gel polymer electrolyte (GPE) is reported in this paper. In this GPE, blending polymer of poly(ethylene oxide) (PEO) with poly(vinylidene fluoride-hexafluoropropylene) (P(VdF-HFP)), doped with nano-Al_2O_3 and supported by polypropylene (PP), is used as polymer matrix, namely PEO–P(VdF-HFP)–Al_2O_3/PP. The performances of the PEO–P(VdF-HFP)–Al_2O_3/PP membrane and the corresponding GPE are characterized with mechanical test, CA, EIS, TGA and charge–discharge test. It is found that the performances of the membrane and the GPE depend to a great extent on the content of doped nano-Al_2O_3. With doping 10 wt.% nano-Al_2O_3 in PEO–P(VdF-HFP), the mechanical strength from 9.3 MPa to 14.3 MPa, the porosity of the membrane increases from 42% to 49%, the electrolyte uptake from 176% to 273%, the thermal decomposition temperature from 225 °C to 355 °C, and the ionic conductivity of corresponding GPE is improved from 2.7×10^{-3} S cm^{-1} to 3.8×10^{-3} S cm^{-1}. The lithium ion battery using this GPE exhibits good rate and cycle performances.

1. Introduction

In the past decades, lithium ion battery has been widely used in portable electronic devices. Compared to other rechargeable battery, lithium ion battery has many advantages, including high energy density and low environmental pollution, thus is believed to be the most promising power source for electric vehicles that does not use gasoline and has no carbon emission [1]. However, the application of lithium ion battery faces several problems, one of which is safety that results mainly from the use of liquid organic electrolyte [2–5]. Gel polymer electrolyte (GPE), which uses polymer as a matrix to entrap liquid components, is much safer than conventional liquid electrolyte when used in lithium ion batteries [6]. GPE needs good comprehensive performances to meet the demand of lithium ion battery as the power source for electric vehicles. However, it is difficult to balance the different performances of GPE. For example, the GPE that has high ionic conductivity usually lacks mechanical strength.

Polyvinylidene fluoride (PVdF) has been attracting extensive attention for its use as polymer matrix of GPE due to its good affinity to liquid electrolyte and electrochemical stability [7]. Since PVdF tends to crystallize and its crystallites block the transfer of Li^+ ions, the ionic conductivity of PVdF-based GPE is low and thus leads to poor rate performance of lithium ion battery [8]. It is well known that the combination of hexafluoropropylene (HFP) with VdF forming P(VdF-HFP) results in lower crystallinity of the polymer [9]. Furthermore, the performance of P(VdF-HFP) can be improved by its blending with poly(ethylene oxide) (PEO). However, the performances of this PEO–P(VdF-HFP) are not good enough for its application in lithium ion battery. For example, the ionic conductivity of the polymer electrolyte with a blend of PEO and P(VDF-HFP) as host polymer, a mixture of ethylene carbonate (EC) and propylene carbonate (PC) as solvent and $LiClO_4$ as salt at 30 °C is 1.3×10^{-4} S cm^{-1} and its mechanical strength is only 3.5 MPa [10].

The poor performance of GPE can be improved to some extent by doping inorganic particles into the polymer matrix, such as aluminum oxyhydroxide, nano-SiO_2 [11–14]. And the mechanical strength of GPE can be obviously improved by using a support,

* Corresponding author at: School of Chemistry and Environment, South China Normal University, Guangzhou 510006, China. Tel.: +86 20 39310256; fax: +86 20 39310256.
E-mail address: liwsh@scnu.edu.cn (W.S. Li).

0378-7753/$ – see front matter © 2010 Elsevier B.V. All rights reserved.
doi:10.1016/j.jpowsour.2010.10.062

such as polyethylene (PE), polypropylene (PP) or non-woven fabrics [15,16].

In this paper, a new GPE, PEO–P(VdF-HFP)–Al_2O_3/PP based GPE, was prepared by using the blending polymer of PEO and P(VdF-HFP) as the polymer matrix that was doped with nano-Al_2O_3 and supported by PP. The characterizations of comprehensive performances indicate that this GPE exhibits high mechanical strength as well as high ionic conductivity and the lithium ion battery using this GPE has good rate capacity and cyclic stability.

2. Experimental

2.1. Preparation

PEO (Mw ≈ 200,000) and P(VdF-HFP) (Kynar 2801, EIF Atochem) were used as purchased. A certain content of nano-Al_2O_3 (Germany Degussa, average particle size of 100 nm, used as purchased without further purification) was dispersed in acetone solution, then PEO and P(VdF-HFP), with the mass ratio of 1:1, were dissolved in above acetone solution at a concentration of 4 wt.% at 40 °C for 5 h under ultrasonication to form viscous slurry. A microporous PP separator (Celgard A273, USA, thickness: 16 μm) was immersed in the slurry for 1 h, taken out and dried in the air atmosphere for 1 h and then in the vacuum at 50 °C for 24 h, the PEO–P(VdF-HFP)–Al_2O_3/PP based membranes were obtained. The PEO–P(VdF-HFP)–Al_2O_3 polymer was coated onto both sides of the PP separator after dipping process and the thickness of the final membrane increased from 16 μm to 26 μm with the mass ratio of PP: (PEO + PVDF-HFP–Al_2O_3) being about 1:1. All the samples used in this paper were prepared under the same conditions.

To prepare GPEs, the PEO–P(VdF-HFP)–Al_2O_3/PP based membranes were immersed in an electrolyte solution, 1 M $LiPF_6$ in ethylene carbonate (EC)/dimethyl carbonate (DMC)/ethylmethyl carbonate (EMC) (1:1:1 in volume, from Dongguan Shanshan Battery Materials Co. Ltd., battery grade) in an argon-filled glove box (Mikrouna). The PEO–P(VdF-HFP)/PP based GPE without doping nano-Al_2O_3 was also prepared under the same conditions for comparison.

2.2. Characterization

Mechanical strength measurements were carried out on a Gotech GT-TS-2000 apparatus at a crosshead speed of 100 mm min^{-1}, using standard dumb bell type tensile bars for testing the samples at room temperature. The elongation length was measured during the deformation.

In order to measure the porosity, the PEO–P(VdF-HFP)–Al_2O_3/PP based membranes with different content of nano-Al_2O_3 were immersed into *n*-butanol for 2 h. The porosity (*P*) was calculated by Eq. (1).

$$P = \frac{m_a/\rho_a}{(m_a/\rho_a) + (m_p/\rho_p)} \quad (1)$$

where ρ_a and ρ_p are the density of *n*-butanol and the dry membrane, respectively; m_a and m_p are the mass of the *n*-butanol-incorporated membrane and the dry membrane, respectively.

The rectangular membrane (34 mm × 45 mm × 0.026 mm) was used to determine the electrolyte uptake (*A*) of PEO–P(VdF-HFP)–Al_2O_3/PP based membranes. The samples were immersed in 1 M $LiPF_6$ (EC/DMC/EMC) (1:1:1 in volume) electrolyte for 0.5 h in a glove box filled with dry argon (Mikrouna). After activation, the membranes were removed from the liquid electrolyte and the excess electrolyte on the surface was removed by pressing lightly between two sheets of filter paper. The electrolyte uptake or the percentage increase in weight was calculated by Eq. (2).

$$A(\%) = \frac{W_2 - W_1}{W_1} \times 100\% \quad (2)$$

where W_1 is the weight of the dry membrane and W_2 is the weight of wet membrane after absorbing liquid electrolyte.

The thermal stability of the membrane was analyzed with thermogravimetric analyzer (NETZSCH STA 409 PC/PG). The compatibility of PEO–P(VdF-HFP)–Al_2O_3/PP based GPE with lithium metal anode was understood by electrochemical impedance spectra (EIS) using the symmetrical cell Li/GPE/Li with potential amplitude of 5 mV from 500 kHz to 30 mHz. The lithium ion transference number was measured by the combination of chronoamperometry (CA) and EIS using symmetrical cell Li/GPE/Li. It can be obtained according to Eq. (3) that was introduced by Bruce and co-workers [17,18].

$$t_+ = \frac{I_S(\Delta V - I_0R_0)}{I_O(\Delta V - I_SR_S)} \quad (3)$$

where $\triangle V$ is the potential applied to the cell in CA (the used $\triangle V$ was 10 mV in this work), I_0 is the initial current, I_S is the steady-state current, R_0 is the charge transfer resistance before polarization, and R_S is the steady-state charge transfer resistance after polarization. The charge transfer resistances were determined by EIS.

The ionic conductivity of GPE was determined by the symmetrical cell stainless steel (SS)/GPE/SS using EIS with potential amplitude of 5 mV from 500 kHz to 1 Hz. GPE was sandwiched between two SS discs (diameter Φ = 14 mm). The ionic conductivity was calculated from the bulk electrolyte resistance (*R*) according to Eq. (4).

$$\sigma = \frac{l}{RS} \quad (4)$$

where *l* is the thickness of the GPE, *S* is the contact area between GPE and SS disc. The bulk electrolyte resistance was obtained from the complex impedance diagram.

To understand the charge–discharge performance of lithium ion battery using the prepared GPE, the cells Li/GPE/$LiCoO_2$ and Li/GPE/graphite were set up and charge–discharge test was carried out using Land Battery Test System (Wuhan Land Electronic Co. Ltd.). In the preparation of $LiCoO_2$ electrode, $LiCoO_2$ (provided by Amperex Technology Limited, Dongguan) was used as the active material and carbon black (Super P, MMM carbon, Belgium) was used as a conductive agent while PVdF was used as a binder with a weight ratio of 90:5:5. N-methylpyrrolidone (NMP) was used as solvent to prepare the electrode slurry that was then coated on an Al foil. The obtained thickness of the $LiCoO_2$ electrode was about 49 μm (Al foil: 14 μm). In the preparation of graphite electrode, the commercial graphite (provided by Amperex Technology Limited, Dongguan) was used as the active material, carbon black (Super P) was used as a conductive agent, styrene-butadiene rubber (SBR) and carboxymethyl cellulose (CMC) were used as binder with the mass ratio of 94.5:1.5:2.5:1.5. Deionized water was used as solvent to prepare the electrode slurry that was then coated on a Cu foil. The obtained thickness of the graphite electrode was about 82 μm (Cu foil: 11 μm). Both electrodes were cut into the disc with an area of 1.54 cm^2 for 2032 coin cell use. The $LiCoO_2$ electrode had a theoretic capacity of about 2.4 mAh while the graphite electrode had about 5.6 mAh for each disc.

3. Results and discussion

3.1. Effect of nano-Al_2O_3 on mechanical strength

For both the industrial assembling feasibility and practical application safety, the mechanical strength is the key factors [19]. Fig. 1

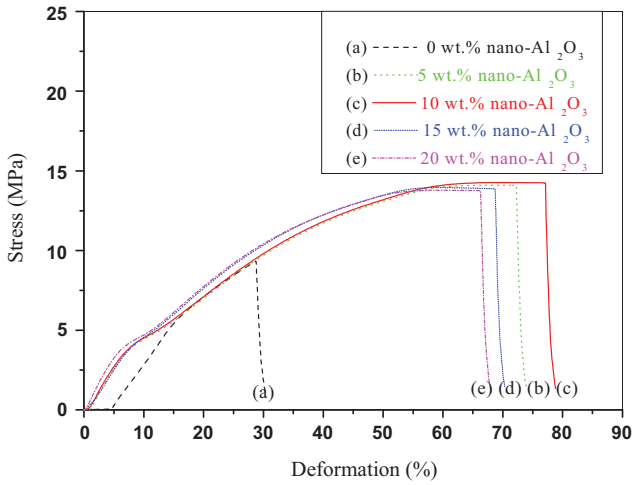

Fig. 1. The relation of engineering stress and engineering deformation of PEO–P(VdF-HFP)–Al_2O_3/PP based membranes with different contents of nano-Al_2O_3.

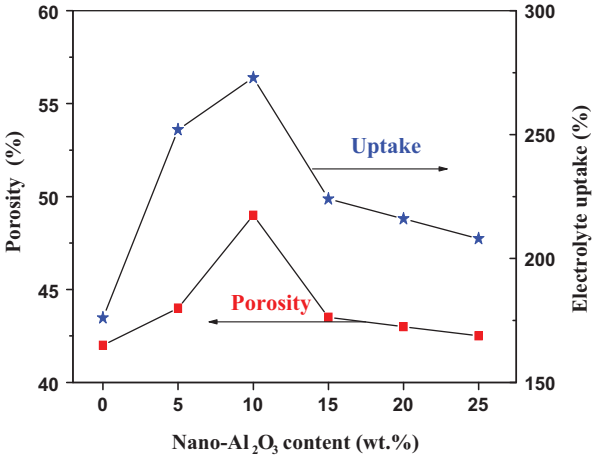

Fig. 2. The dependence of porosity and electrolyte uptake of PEO–P(VdF-HFP)–Al_2O_3/PP based membranes on the content of nano-Al_2O_3.

presents the stress curves of PEO–P(VdF-HFP)–Al_2O_3/PP based membranes with different contents of nano-Al_2O_3. As can be seen from Fig. 1, the fracture strength of the membrane without nano-particle is 9.3 MPa, which is significantly higher than the blended polymer PEO–P(VdF-HFP) based membrane without supporter (only 3.5 MPa) [10]. When adding nano-Al_2O_3 into PEO–P(VdF-HFP), obvious improvement can be observed although there is less difference in fracture strength for the membranes containing different contents of nano-Al_2O_3. The highest fracture stress is 14.3 MPa for the 10 wt.% nano-Al_2O_3 membrane. This value is far higher than the poly(acrylonitrile-methyl methacrylate) membrane and is nearly the same as the poly(acrylonitrile-butyl acrylate) membrane [19]. Although the thickness of the membranes is different, based on the formula: $p = F/S$, where p is the mechanical strength (units: MPa), F is the force applied into the membrane (units: N) and S is the sample area (units: mm^2), the obtained mechanical strength is independent of the thickness and therefore can be used for comparison between the membranes with different thickness. This suggests that adding nano-Al_2O_3 to the membrane during the phase transfer process does not decrease but enhance the mechanical strength of membrane. Nano-Al_2O_3 acts as temporary mechanical connection point, which helps to form the net structure and connects firmly with the PEO and P(VdF-HFP) polymer in the blending system. The effective connection points are related to the content of nano-Al_2O_3. Increasing or reducing the content of nano-Al_2O_3 might reduce the effective connection point, resulting in the lower mechanical strength. The increasing of mechanical strength resulted from the use of nano-Al_2O_3 improves the morphological structure of the membrane, providing polymer with enhanced performances for its applications in polymer lithium ion batteries. Such mechanical strength enhancement has also been observed for other polymer membranes, such as PVdF/nano-SiO_2 [20], PVdF/TiO_2 [21] and P(VdF-HFP)/Sb_2O_3 [22].

3.2. Effect of nano-Al_2O_3 on porosity and electrolyte uptake

Fig. 2 presents the dependence of porosity and electrolyte uptake of PEO–P(VdF-HFP)–Al_2O_3/PP based membranes on the different contents of nano-Al_2O_3. It can be seen from Fig. 2 that the porosity and the electrolyte uptake of the membranes are affected by doping nano-Al_2O_3. The porosity and the electrolyte uptake have similar dependence on the doped content of nano-Al_2O_3. Both increases with increasing the content of nano-Al_2O_3, reaches the maximum at 10 wt.% nano-Al_2O_3 and then decreases with increasing the content of nano-Al_2O_3 further. Similar phenomenon was observed when nano-Al_2O_3 was doped into poly(acrylonitrile-methyl methacrylate) [23]. Due to the interaction between nano-Al_2O_3 and the polymer, the pore structure of the membrane has been improved. Higher porosity leads to the higher electrolyte uptake [24]. The porosity of the membrane with 10 wt.% nano-Al_2O_3 is 49% compared to 42% of the membrane without nano-Al_2O_3, while the electrolyte uptake of the membrane with 10 wt.% nano-Al_2O_3 calculated by the Eq. (2) is 273% (the weight of the sample after absorbing liquid electrolyte increases from 16.2 mg to 44.3 mg) compared to 176% (increases from 16.2 mg to 28.5 mg) of the membrane without doping nano-Al_2O_3. The electrolyte uptakes of the membranes depend greatly on their pore structure. Higher electrolyte uptake means higher concentration of Li^+ ions in the membrane and larger porosity facilitates the transfer of Li^+ ions because of increasing the number of transport channels [25]. Thus the doping of nano-Al_2O_3 in PEO–P(VdF-HFP) should contribute to the improvement in ionic conductivity of GPE.

3.3. Effect of nano-Al_2O_3 on lithium ion transference number

The lithium ion transference number (t_+) in GPE is one of the most important parameters that determine the carrier migration properties of lithium ion battery. The ideal value of t_+ is one, since the t_+ lower than one would tend to develop concentration gradients during charge–discharge cycling at electrode surfaces and lead to limiting currents [26]. However, since the interaction between solvent molecules and lithium ions in electrolyte affords a fraction of conductivity, the t_+ in electrolyte is far lower than one.

Fig. 3 presents the lithium ion transference number of PEO–P(VdF-HFP)–Al_2O_3/PP based GPEs with different contents of nano-Al_2O_3. The ion transference number was obtained based on Eq. (3). It can be seen from Fig. 3 that all the GPEs doped with nano-Al_2O_3 have higher t_+ than the GPE without nano-Al_2O_3, which is 0.52. And the GPE with 10 wt.% nano-Al_2O_3 has the largest t_+, 0.62, which is higher than the values that was reported in most of literatures [4,8,27–31] and competitive to the highest value that has been reported [32–34]. This suggests that the doping of nano-Al_2O_3 in PEO–P(VdF-HFP) contributes more effectively to the improvement in ionic conductivity of the corresponding GPE than other methods and this GPE is more suitable for use in lithium ion battery than the GPEs based on other polymers.

The effect of nano-Al_2O_3 on ionic conductivity results from Lewis acid-base reactions between the nano-particle and the PEO–P(VdF-HFP) segments. Nano-Al_2O_3 competes with lithium

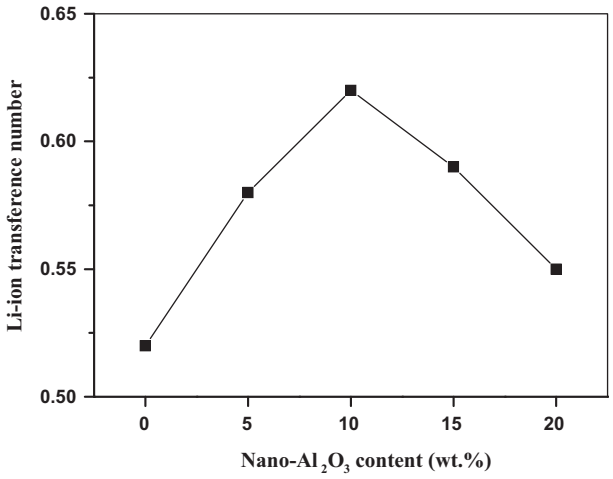

Fig. 3. The dependence of lithium ion transference number of PEO–P(VdF-HFP)–Al_2O_3/PP based GPEs on the contents of nano-Al_2O_3.

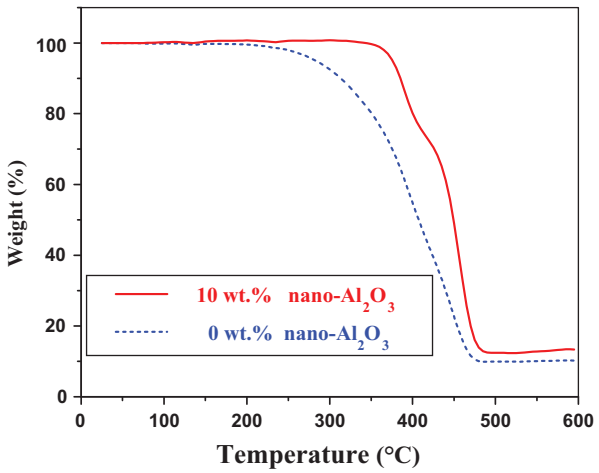

Fig. 4. TG curves of PEO–P(VdF-HFP)–Al_2O_3/PP based membranes without and with 10 wt.% nano-Al_2O_3.

cations as Lewis acid for the formation of complexes of PEO–P(VdF-HFP). Thus, the nano-particle acts as cross-linking centers for the polymer segments, lowering the polymer chain reorganization tendency and promoting an overall structure stiffness. Such a structure modification provides lithium ion conducting pathways at the high surface area of the nano-particles and shortens the Li^+ ion transport distance, resulting in the improvement of Li^+ ion transference number. The interactions of Lewis-acidic Al_2O_3 with PF_6^- anions lead to the liberation of higher amounts of free Li^+ and the increase of Li^+ transference number. It is obvious that when the content of nano-Al_2O_3 is larger than 10 wt.%, the contribution of nano-Al_2O_3 will be reduced.

By comparing Fig. 2 with Fig. 3, it can be found that porosity, electrolyte uptake and lithium ion transference number have the same tendency, i.e. all the membranes based GPEs containing nano-particle have higher value than the membrane that without any nano-particle, and the membrane with 10 wt.% nano-Al_2O_3 has the best performances. Higher porosity leads to higher electrolyte, thus higher lithium ion transference number. It can be expected that the improved pore structure of the membrane due to doping appropriate amount of nano-Al_2O_3 will benefit to the ionic conductivity of the PEO–P(VdF-HFP)–Al_2O_3/PP based GPE.

From the above results, it can be found that PEO–P(VdF-HFP)–Al_2O_3/PP based membrane with 10 wt.% nano-Al_2O_3 exhibits the best performance. Therefore, in the next discussions, we only compare the membranes and the GPEs with 0 wt.% and 10 wt.% nano-Al_2O_3.

3.4. Thermal stability of membranes

Fig. 4 presents the TG curves of PEO–P(VdF-HFP)–Al_2O_3/PP based membranes with 0 wt.% and 10 wt.% nano-Al_2O_3, obtained under N_2 atmosphere from room temperature to 600 °C at a heating rate of 10 °C min^{-1}. Here, we define the decomposition temperature of a polymer at which it losses its weight larger than 1 wt.% of its original weight. The PEO–P(VdF-HFP)/PP based membrane has high thermal stability, which can be stable up to 225 °C. When adding 10 wt.% nano-Al_2O_3 to the PEO–P(VdF-HFP)/PP based membrane, it can be seen from Fig. 4 that the shape of TG curve of the membrane is similar to that of the membrane without nano-Al_2O_3, but the decomposition temperature is significantly improved from 225 °C to 355 °C. Under heating, copolymer in the membrane decomposes through the breakdown of the C–C and C–H bonds in the copolymer matrix, forming gaseous compounds (CO_2 and H_2O) and losing its weight. The improvement of thermal durability of the membrane due to doping nano-Al_2O_3 can be ascribed to the improved bond strength of the copolymer in the doped membrane, which is consistent with the mechanical strength analysis. It suggests that doping nano-Al_2O_3 into PEO–P(VdF-HFP)/PP based membrane does improve the thermal stability of the membrane.

3.5. Interfacial stability

Compatibility with electrode is an essential factor for the safety and cyclic performance in lithium ion batteries. The interfacial stability of PEO–P(VdF-HFP)–Al_2O_3/PP based GPEs with lithium metal anode is understood by their interfacial resistance, which is associated with the passive layer and the charge transfer resistances on the lithium metal electrode [35]. In order to get the interfacial resistance between GPE and lithium metal, electrochemical impedance spectrum (EIS) of the cell Li/GPE/Li at open circuit was monitored with time [15].

Fig. 5 shows the EIS of the symmetrical cell Li/GPE/Li for different time. It can be seen from Fig. 5(a) that the interfacial resistance of the membrane without nano-Al_2O_3 increases from 68 Ω cm^2 on the first day to 98 Ω cm^2 after the 20 days. However, the increased magnitude for the membrane with 10 wt.% nano-Al_2O_3 seems much lower, from 41 Ω cm^2 on the first day to 66 Ω cm^2 after the 20 days, as shown in Fig. 5(b). The interfacial resistance of the cell using the membrane without the nano-Al_2O_3 increases further but the cell using the membrane with 10 wt.% nano-Al_2O_3 keeps almost unchanged after the 20 days. This indicates that passive film forms on lithium electrode at the beginning and does not change as soon as it is formed when adding nano-Al_2O_3 to the membrane, thus the GPE with nano-Al_2O_3 exhibits good compatibility with lithium electrode. The nano-particle filler with high surface area can hold the solvent effectively due to the capillary force, and reduce the growth rate of the resistive layer on the Li electrode surface. On the other hand, nano-Al_2O_3 helps to trap residual trace of impurities such as water and oxygen, so the reaction between the impurities and the lithium metal is inhibited, leading to the improvement in the compatibility of the GPE with lithium electrode [36–38].

3.6. Ionic conductivity

Fig. 6 presents the reciprocal temperature dependence of the ionic conductivity for PEO–P(VdF-HFP)–Al_2O_3/PP based GPEs. Calculated by Eq. (4), the ionic conductivity of PEO–P(VdF-HFP)–Al_2O_3/PP based GPE with 10 wt.% nano-Al_2O_3 is 3.8×10^{-3} S cm^{-1} while the GPE without nano-Al_2O_3 is only

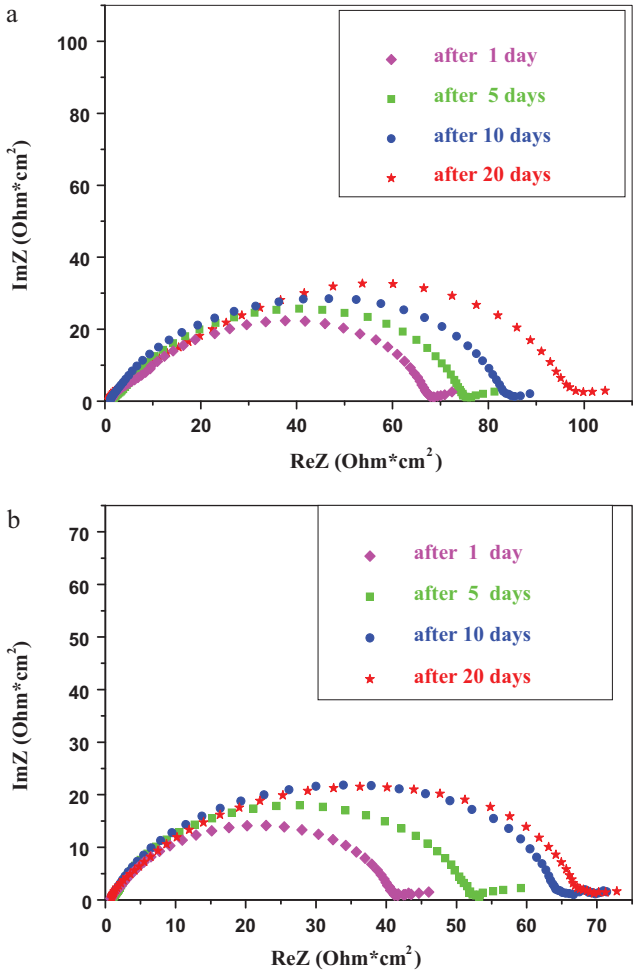

Fig. 5. Electrochemical impedance spectra of the cell Li/GPE/Li, (a): without nano-Al_2O_3, (b): with 10 wt.% nano-Al_2O_3.

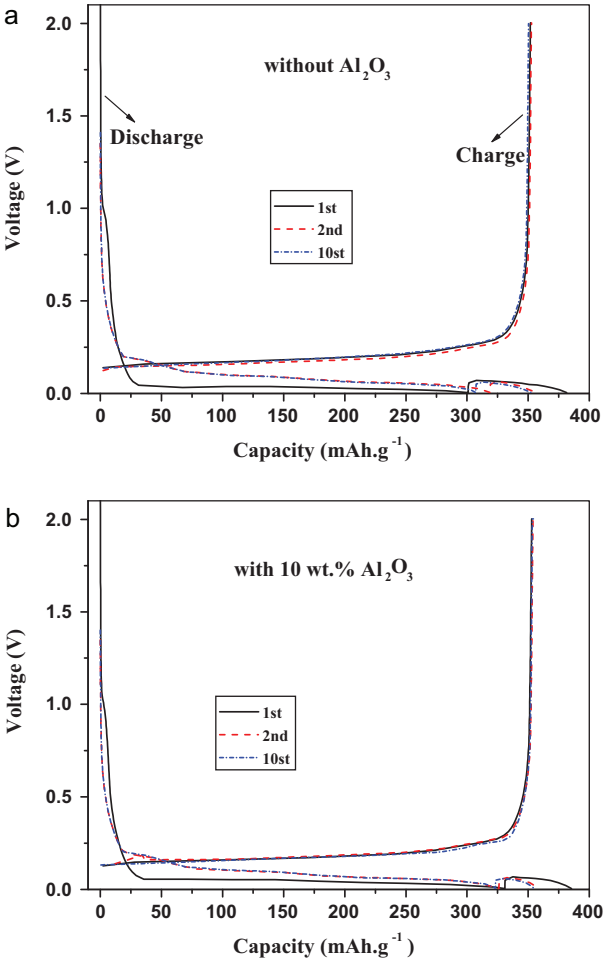

Fig. 7. Charge–discharge curves of the cell Li/GPE/graphite for the 1st, 2nd and 10th cycle, (a): without Al_2O_3, (b): with 10 wt.% Al_2O_3. The cell was discharged at 0.05 C (0.29 mA) from 2 V to 0.005 V and then at 0.05 mA to 0.005 V, and charged at 0.1 C (0.58 mA) from 0.005 V to 2 V.

2.7×10^{-3} S cm^{-1} at room temperature. Based on the results obtained from the effect of the doping nano-Al_2O_3 on electrolyte uptake (Section 3.2), it can be concluded that the increase in conductivity is mainly due to the more liquid electrolyte in the GPE with doping nano-Al_2O_3.

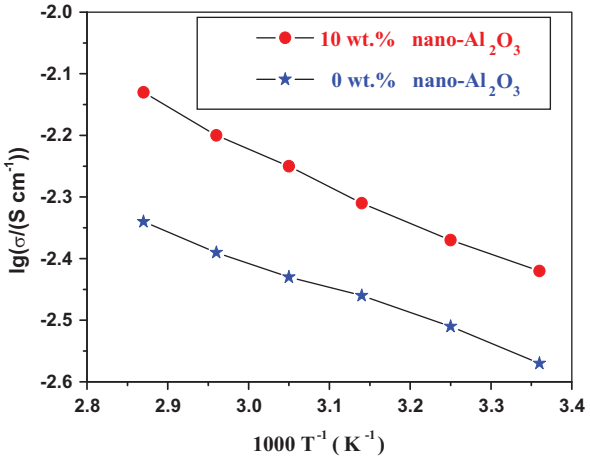

Fig. 6. Temperature dependence of ionic conductivity for PEO–P(VdF-HFP)–Al_2O_3/PP based GPEs with 0 wt.% and 10 wt.% nano-Al_2O_3.

In order to further understand the conductivity mechanism of PEO–P(VdF-HFP)–Al_2O_3/PP based GPEs, the ionic conductivity of the GPEs with 0 wt.% and 10 wt.% nano-Al_2O_3 is determined under different temperature. It can be seen in Fig. 6 that the ionic conductivity of the GPEs with 0 wt.% and 10 wt.% nano-Al_2O_3 have the same dependence on the reciprocal temperature, i.e. the ionic conductivity increases with the reciprocal temperature. As the temperature increases, the polymer tends to produce more free volume by expanding, resulting in the enhancement of the ionic and polymer segmental mobility. However, the ionic conductivity is not related linearly to the reciprocal temperature, suggesting that doping nano-Al_2O_3 does not change the conductive mechanism of the PEO–P(VdF-HFP)–Al_2O_3/PP based GPEs, and obeys the Vogel–Tamman–Fulcher (VTF) equation reflecting the transport properties in a viscous matrix. This behavior is characteristic of the amorphous polymeric electrolytes that follow free-volume model, and the ionic transport mechanism is governed by the free-volume-theory [39–41].

3.7. Rate and cycle performance

Fig. 7 presents the charge–discharge curves of the cell Li/GPE/graphite for the 1st, 2nd and 10th cycle. It can be found from Fig. 7 that the charge capacity of the cell using the GPE without doping Al_2O_3 is 352 mAh g^{-1} with a coulombic efficiency of 92% (defined as the ratio of the charge capacity to the discharge capac-

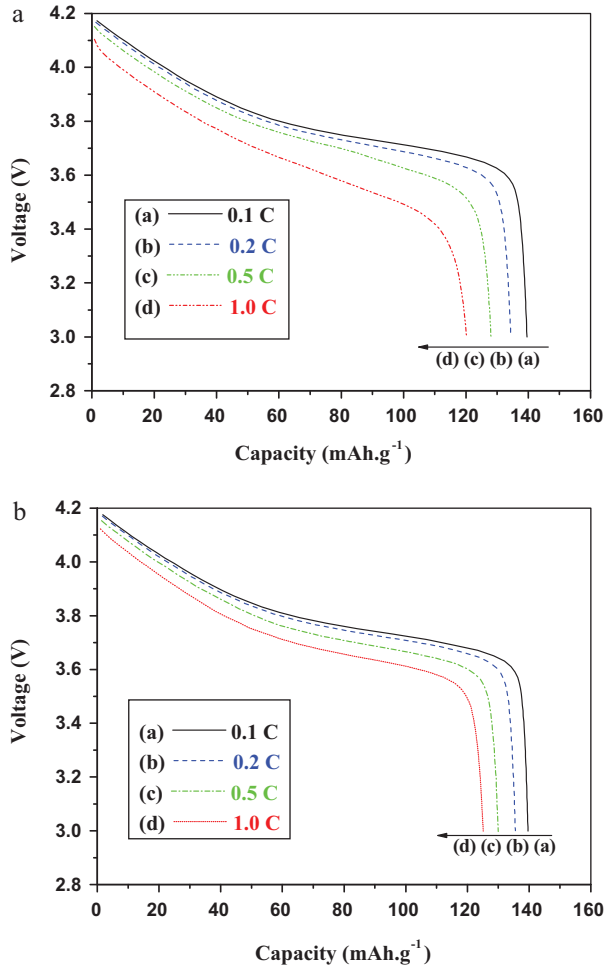

Fig. 8. Rate discharge performance of the cell Li/GPE/$LiCoO_2$ from 4.2 V to 3.0 V, (a): without nano-Al_2O_3, (b): with 10 wt.% nano-Al_2O_3. The cell was charged at 0.1 C from 3.0 V to 4.2 V and discharged at 0.1 C, 0.2 C, 0.5 C, and 1.0 C.

ity) for the 1st cycle and 350 mAh g^{-1} with the coulombic efficiency of 99% for the 10th cycle, while the charge capacity of the cell using the GPE with doping is 353 mAh g^{-1} with the coulonmic efficiency of 92% for the 1st cycle and 353 mAh g^{-1} with the coulombic efficiency of 100% for the 10th cycle. It is obvious that the GPE doped with nano-Al_2O_3 is good for use in the lithium ion battery using graphite as anode.

Fig. 8 presents the discharge curves of the cell Li/GPE/$LiCoO_2$ at different rates (0.1 C, 0.2 C, 0.5 C and 1.0 C). It can be seen from Fig. 8 that the discharge capacity of the cell is gradually faded with increasing discharge rate but keeps relatively high. The cells at 0.1 C achieve a high capacity, 140 mAh g^{-1} for the cell with 10 wt.% nano-Al_2O_3 and 139 mAh g^{-1} for the cell without nano-Al_2O_3. At 1.0 C, the capacity keeps 89.6% of that at 0.1 C for the cell with 10 wt.% nano-Al_2O_3 (Fig. 8(b)), but only 86.1% for the cell without nano-Al_2O_3 (Fig. 8(a)). Therefore, the GPE doped with nano-Al_2O_3 is also good for use in the lithium ion battery using $LiCoO_2$ as cathode.

Fig. 9 presents the cyclic performance of the cell Li/GPE/$LiCoO_2$. As can be seen from Fig. 9 that the cell without nano-Al_2O_3 has the initial capacity as high as the battery with 10 wt.% nano-Al_2O_3. After 50 cycles, the cell with 10 wt.% nano-Al_2O_3 keeps 87.2% of its initial discharge capacity but the cell without nano-Al_2O_3 keeps only 82.8% of its initial discharge capacity. Thus, the cycling performance of the cell using PEO–P(VdF-HFP)–Al_2O_3/PP as GPE is also improved. The doping of nano-Al_2O_3 in polymer matrix improves the rate and cycle performance of lithium ion battery, which should

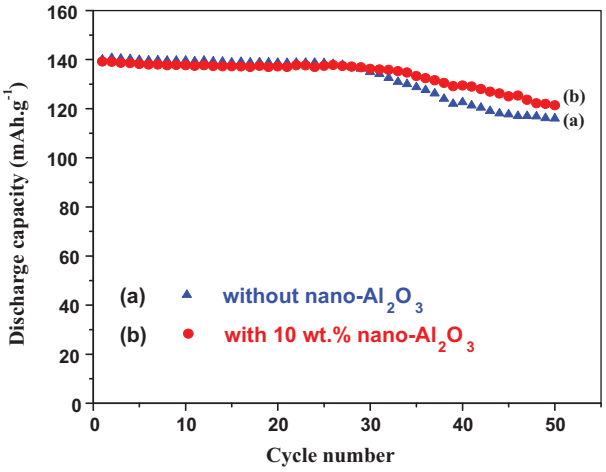

Fig. 9. Cyclic stability of the cell Li/GPE/$LiCoO_2$, charged and discharged at 0.2 C between 4.2 V and 3.0 V, (a): without nano-Al_2O_3, (b): with 10 wt.% nano-Al_2O_3.

be ascribed to the higher ionic conductivity of the GPE and its better compatibility with electrodes [42].

4. Conclusions

A new gel polymer electrolyte (GPE), PEO–P(VdF-HFP)–Al_2O_3/PP based GPE, is reported in this work. It is found that the nano-Al_2O_3 can effectively improve the performance of the polymer membrane and the corresponding GPE. When doping of 10 wt.% nano-Al_2O_3 in PEO–P(VdF-HFP)–Al_2O_3/PP, the membrane exhibits best mechanical strength and the corresponding GPE shows good rate capacity and cyclic stability. The enhanced mechanical strength can be ascribed to the function of nano-Al_2O_3 as temporary mechanical connection point, helps to form the net structure and connects firmly with the PEO and P(VdF-HFP) polymer in the blending system. The improved rate and cycle performance can be ascribed to the higher ionic conductivity of the GPE doped with nano-Al_2O_3 and its better compatibility with electrodes.

Acknowledgements

The authors are highly grateful for the financial support from National Natural Science Foundation of China (NNSFC, 20873046), Specialized Research Fund for the Doctoral Program of Higher Education (Grant No. 200805740004) and Guangdong Province Nature Science Foundation (Grant No. 9451063101002082).

References

[1] W.H. Yao, Z.R. Zhang, J. Gao, J. Li, J. Xu, Z.C. Wang, Y. Yang, Energy Environ. Sci. 2 (2009) 1102.
[2] M.M. Rao, J.S. Liu, W.S. Li, Y. Liang, Y.H. Liao, L.Z. Zhao, J. Power Sources 189 (2009) 711.
[3] D.Y. Zhou, G.Z. Wang, W.S. Li, G.L. Li, C.L. Tan, M.M. Rao, Y.H. Liao, J. Power Sources 184 (2008) 477.
[4] Y.H. Liao, D.Y. Zhou, M.M. Rao, W.S. Li, Z.P. Cai, Y. Liang, C.L. Tan, J. Power Sources 189 (2009) 139.
[5] L. Lu, X.X. Zuo, W.S. Li, J.S. Liu, M.Q. Xu, Acta Chim. Sinica 65 (2007) 475.
[6] G.C. Li, Z.H. Li, P. Zhang, H.P. Zhang, Y.P. Wu, Pure Appl. Chem. 80 (2008) 2553.
[7] Z. Jiang, B. Carroll, K.M. Abraham, Electrochim. Acta 42 (1997) 2667.
[8] A.I. Gopalan, P. Santhosh, K.M. Manesh, J.H. Nho, S.H. Kim, C.G. Hwang, K.P. Lee, J. Membr. Sci. 325 (2008) 683.
[9] Z.H. Li, H.P. Zhang, P. Zhang, G.C. Li, Y.P. Wu, X.D. Zhou, J. Membr. Sci. 322 (2008) 416.
[10] L.Z. Fan, Z.M. Dang, C.W. Nan, M. Li, Electrochim. Acta 48 (2002) 205.
[11] P.P. Prosini, P. Villano, M. Carewska, Electrochim. Acta 48 (2002) 227.
[12] D. Świerczyński, A. Zalewska, W. Wieczorek, Chem. Mater. 13 (2001) 1560.
[13] J.Y. Xi, X.P. Qiu, M.Z. Cui, X.Z. Tang, W.T. Zhu, L.Q. Chen, J. Power Sources 156 (2006) 581.

[14] J.Y. Xi, X.P. Qiu, L.Q. Chen, Solid State Ionics 177 (2006) 709.
[15] M.M. Rao, J.S. Liu, W.S. Li, Y. Liang, D.Y. Zhou, J. Membr. Sci. 322 (2008) 314.
[16] M.K. Song, Y.T. Kim, J.Y. Cho, B.W. Cho, B.N. Popov, H.W. Rhee, J. Power Sources 125 (2004) 10.
[17] P.G. Bruce, C.A. Vincent, J. Electroanal. Chem. 225 (1987) 1.
[18] J. Evans, C.A. Vincent, P.G. Bruce, Polymer 28 (1987) 2324.
[19] Z. Tian, X.M. He, W.H. Pu, C.R. Wan, C.Y. Jiang, Electrochim. Acta 52 (2006) 688.
[20] D. Shah, P. Maiti, E. Gunn, D.F. Schmidt, D.D. Jiang, C.A. Batt, E.P. Giannelis, Adv. Mater. 16 (2004) 1173.
[21] Y.J. Wang, D. Kim, Electrochim. Acta 52 (2007) 3181.
[22] V. Aravindan, P. Vickraman, Solid State Sci. 9 (2007) 1069.
[23] M.M. Rao, J.S. Liu, W.S. Li, Y.H. Liao, Y. Liang, L.Z. Zhao, J. Solid State Electrochem. 14 (2009) 255.
[24] M. Nookala, B. Kumar, S. Rodrigues, J. Power Sources 111 (2002) 165.
[25] P. Zhang, H.P. Zhang, G.C. Li, Z.H. Li, Y.P. Wu, Electrochem. Commun. 10 (2008) 1052.
[26] F.B. Dias, L. Plomp, J.B.J. Veldhuis, J. Power Sources 88 (2000) 169.
[27] Y.H. Liao, M.M. Rao, W.S. Li, C.L. Tan, J. Yi, L. Chen, Electrochim. Acta 54 (2009) 6396.
[28] S. Panero, B. Scrosati, H.H. Sumathipala, W. Wieczorek, J. Power Sources 167 (2007) 510.
[29] A. Manuel Stephan, T. Kee Suk Nahm, M. Prem Kumar, G. Anbu Kulandainathan, J. Ravi, Wilson, J. Power Sources 159 (2006) 1316.
[30] S.H. Chung, Y. Wang, L. Persi, F. Croce, S.G. Greenbaum, B. Scrosati, E. Plichta, J. Power Sources 97–98 (2001) 644.
[31] M. Stolarska, L. Niedzicki, R. Borkowska, A. Zalewska, W. Wieczorek, Electrochim. Acta 53 (2007) 1512.
[32] Z.H. Li, P. Zhang, H.P. Zhang, Y.P. Wu, X.D. Zhou, Electrochem. Commun. 10 (2008) 791.
[33] M. Sivakumar, R. Subadevi, S. Rajendran, H.-C. Wu, N.-L. Wu, Eur. Polym. J. 43 (2007) 4466.
[34] Y.W. Chen-Yang, Y.L. Wang, Y.T. Chen, Y.K. Li, H.C. Chen, H.Y. Chiu, J. Power Sources 182 (2008) 340.
[35] Y. Aihara, S. Arai, K. Hayamizu, Electrochim. Acta 45 (2000) 1321.
[36] C.M. Yang, H.S. Kim, B.K. Na, K.S. Kum, B.W. Cho, J. Power Sources 156 (2006) 574.
[37] Y.X. Jiang, Z.F. Chen, Q.C. Zhuang, J.M. Xu, Q.F. Dong, L. Huang, S.G. Sun, J. Power Sources 160 (2006) 1320.
[38] V. Gentili, S. Panero, P. Reale, B. Scrosati, J. Power Sources 170 (2007) 185.
[39] A.M. Christie, L. Christie, C.A. Vincent, J. Power Sources 74 (1998) 77.
[40] S. Ahmad, T.K. Saxena, S. Ahmad, S.A. Agnihotry, J. Power Sources 159 (2006) 205.
[41] A.M.M. Ali, N.S. Mohamed, A.K. Arof, J. Power Sources 74 (1998) 135.
[42] S.S. Zhang, M.H. Ervin, K. Xu, T.R. Jow, Electrochim. Acta 49 (2004) 3339.